Available online at www.sciencedirect.com
SCIENCE DIRECT
Diamond & Related Materials 14 (2005) 1078–1083
DIAMOND AND RELATED MATERIALS
www.elsevier.com/locate/diamond

Ab initio resonant Raman spectra of diamond-like carbons

S. Piscanec[a,1], F. Mauri[b], A.C. Ferrari[a,*], M. Lazzeri[b], J. Robertson[a]

[a]Engineering Department, University of Cambridge, Trumpington Street, Cambridge, CB2 1PZ, UK
[b]Laboratoire de Mineralogie–Cristallographie de Paris, Universite'Pierre et Marie Curie, Paris, France

Available online 1 February 2005

Abstract

Raman spectroscopy is a standard tool for the characterisation of carbon materials, from graphite to diamond-like carbon and carbon nanotubes. An important factor is the dependence of the Raman spectra on excitation energy, which is due to resonant processes. Here, we calculate the resonant Raman spectra of tetrahedral amorphous carbon. This is done by a tight-binding method, using an approach different from Placzek's approximation, which allows calculation of Raman intensities also in resonant conditions. The calculated spectra confirm that the G peak arises from chains of sp^2 bonded atoms and that it correlates with the atomic and electronic structure of the samples. The calculated dispersion of the G peak position with excitation energy follows the experimental observations. Our ab initio calculations also show that the sp^3 phase can only be seen by using UV excitation above 4 eV, confirming the assignment of the T peak at ~1060 cm^{-1}, seen only in UV Raman measurements, to C–C sp^3 vibrations.

Keywords: Raman spectroscopy; Diamond-like carbon; Electronic properties; Structure

1. Introduction

Amorphous and diamond-like carbons are widely used as protective coating materials [1]. Raman spectroscopy is a fast and non-destructive tool for characterisation of these carbons [2]. All carbons show common features in their Raman spectra in the 800–2000 cm^{-1} region, the so called G and D peaks, which lie at around 1560 and 1360 cm^{-1} respectively for visible excitation, and the T peak at around 1060 cm^{-1}, which becomes visible only for UV excitation [2–10]. The G peak is due to the bond stretching of all pairs of sp^2 atoms in both rings and chains [2]. The D peak is due to the breathing modes of sp^2 atoms in rings [2–6]. The T peak is commonly assigned to the C–C sp^3 vibrations [7–9].

An empirical three-stage model was developed to describe the Raman spectra of carbon films measured at any excitation energy [2,9,10]. The evolution of the Raman spectra is understood by considering an amorphisation trajectory, starting from perfect graphite. The main factor affecting peaks position, width and intensity is the clustering of the sp^2 phase. The sp^2 clustering can in principle vary independently from the sp^3 content, so that for a given sp^3 content and excitation energy, we can have a number of different Raman spectra, or, equivalently, similar Raman spectra for different sp^3 contents. For UV excitation, an increase in clustering always lowers the G peak position. However, in visible Raman the G peak does not depend monotonically on cluster size. If two samples have similar G peak positions in visible Raman but different ones in UV Raman, the sample with the lower G position in the UV has higher sp^2 clustering. A multi-wavelength Raman analysis is thus important to fully characterise the samples. A very useful parameter is then the G peak dispersion Disp(G). This is defined as the slope of the line connecting the G peak positions, measured at different excitation wave-

* Corresponding author. Tel.: +44 1223 332659; fax: +44 1223 332662.
E-mail addresses: sp344@eng.cam.ac.uk (S. Piscanec), acf26@eng.cam.ac.uk (A.C. Ferrari).
[1] Tel.: +44 1223 764093; fax: +44 1223 332662.

0925-9635/$ - see front matter © 2005 Elsevier B.V. All rights reserved.
doi:10.1016/j.diamond.2004.11.043

lengths. Another useful parameter to monitor the carbon bonding is the Full Width at Half Maximum of the G peak, FWHM(G). Both FWHM(G) and Disp(G) always increase as the disorder increases, at every excitation wavelength.

The three-stage model does well describe the evolution of the Raman spectra of any carbon film for any excitation energy. However, a further step is necessary to understand more deeply the physical origin of the Raman spectra of carbon films. This step consists in getting computational tools able to calculate the resonant Raman spectra of any carbon material at any excitation energy. Here we report on the initial development of such a code and we apply it to tetrahedral amorphous carbon. The code is based on tight-binding and implements an approximation, different from Placzek's, which allows calculations of Raman intensities also in resonant conditions. The calculated variation of the G peak position with excitation energy closely follows the experimental G peak dispersion. Our calculations also show that the sp^3 phase can only be seen by using UV excitation above 4 eV, confirming the assignment of the T peak to C–C sp^3 vibrations.

2. Theory of resonant Raman and computational details

The general formula for the Raman intensity consists of terms depending on the vibrational eigenfunctions calculated for the excited Born–Oppenheimer surfaces [11]. The exact calculation of these terms for an amorphous carbon network, such as the one in Fig. 1, which has several tens of atoms in the unit cell [12], is nowadays computationally not possible. The standard approximation used for the Raman intensity calculations in solid-state physics is the so-called Placzek's approximation [13]. In this model, the general expression for the Raman intensity is simplified, and is valid only if the energy of the incoming radiation is smaller than the electronic band gap and no electrons are excited into a real state:

$$I(\mathbf{u},\mathbf{u}_L,\omega) \propto \sum_s \frac{\omega^4}{\omega_s}\left|\frac{\partial\chi(\mathbf{u},\mathbf{u}_L,\omega_L)}{\partial Q_s}\right|^2 (\langle n_s\rangle + 1) \times\delta(\omega-\omega_L+\omega_s) \quad (1)$$

where the index s runs over the normal modes Q_s with frequency ω_s and occupation $<n_s>=\{\exp[\omega_s/(k_BT)-1]\}^{-1}$, ω_L is laser frequency, $\mathbf{u}_L$ and $\mathbf{u}$ are the polarisations of the incident and scattered light and $\chi(\omega_L)$ is the electronic susceptibility. It is clear that Placzek's approximation can be used only for the calculation of Raman intensities in non-resonant conditions. It would thus not work as such for carbon films, where resonance is in principle always present [9,10].

An alternative approximation of the general expression of the Raman intensity was proposed in Ref. [14]. The key assumption is that in a periodic solid with dispersive bands the electronic excitations are generally delocalised, and the excited Born–Oppenheimer surfaces can be simply obtained from a vertical displacement of the ground-state. In this model, the computation of the excited Born–Oppenheimer surfaces is thus greatly simplified. This allows the calculation of Raman spectra also in resonance. The Raman intensity is now given by:

$$I(\omega) \propto \sum_s \rho(n_s)\omega^4|A_s|^2\delta(\omega-\omega_L+\omega_s) \quad (2)$$

where

$$A_s = \sqrt{\frac{n_s+1}{2\omega_s}}\mathbf{q}_s \left.\frac{\partial k(\mathbf{R},\mathbf{R}',\omega_L)}{\partial\mathbf{R}}\right|_{\mathbf{R}=\mathbf{R}'=\mathbf{R}_0^{eq}} \quad (3)$$

where $\mathbf{q}_s$ is the unit vector of the Q_s mode, $\rho(n_s)$ is the probability of finding the system in the state n_s and k is a generalised susceptibility, which reduces to χ of Eq. (1) for

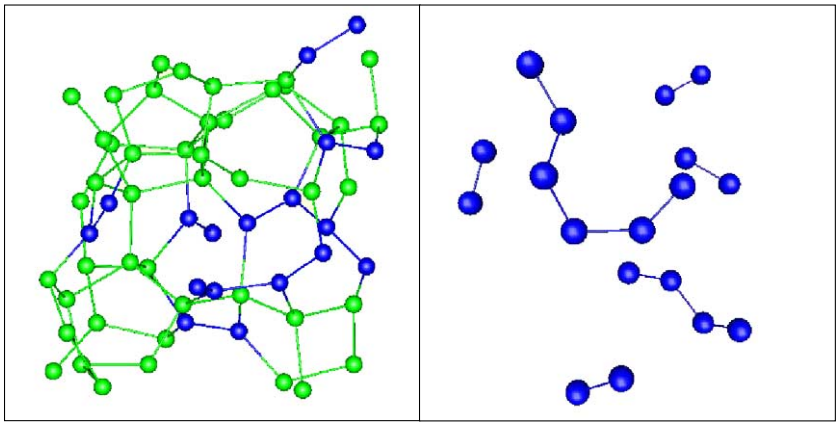

Fig. 1. 64 atoms model ta-C used for the calculations [12].

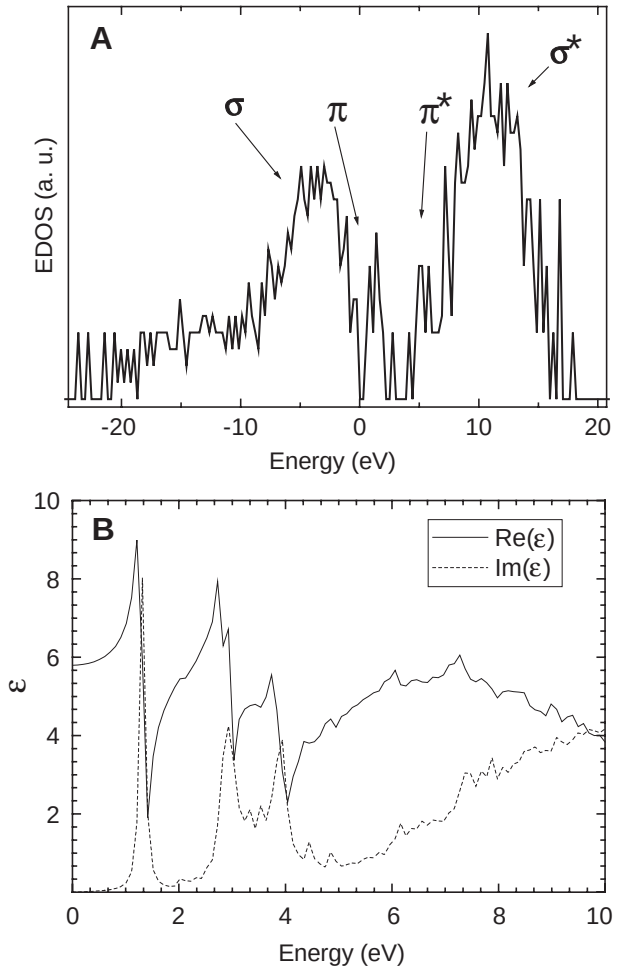

Fig. 2. (A) Calculated electronic density of states of the sample in Fig. 1. The σ and π contributions are indicated. π defect states are present in the gap. The calculated bandgap is 1.4 eV. (B) Calculated electronic dielectric susceptibility. Peaks in Im[$\varepsilon(\omega_L)$], corresponding to electronic transitions between defect states in the gap, are responsible for the anomalous absorption at their energies.

R=R′ [14]. Placzek's approximation can be recovered by performing an additional partial derivative of k (**R, R′**, ω_L) with respect to **R′**.

Here we apply Eq. (2) to the tetrahedral amorphous carbon network of Drabold et al. [12] in Fig. 1. After performing a geometry optimisation, we calculate and analyse its electronic structure and vibrational properties and then we calculate its Raman spectra for excitation wavelengths ranging from 785 to 229 nm.

The geometry optimisation and the calculation of the vibrational properties are performed in the Density Functional Theory (DFT) framework within the Local Density Approximation (LDA) [15], using the Car–Parrinello-Molecular Dynamics (CPMD) code [16]. The electronic wavefunctions are expanded on a planewave basis and the first Brillouin zone is sampled at the Γ point only. The carbon atoms are described by using Troullier–Martins norm-conserving pseudopotentials [17]. In the geometry optimisation, a 50 Ry cut-off energy is used for the expansion of the electronic wavefunctions. The calculation of the dynamical matrix is done by using the finite difference method [16]. Due to its greater computational requirements, the calculation of the Raman intensities is performed within a tight-binding model using s and p orbitals [18].

3. Results and discussion

The Raman spectrum of a material is determined by its electronic and vibrational properties. Thus, in order to obtain reasonable results in the prediction of Raman intensities, we first need to check our ability to calculate both the electronic and vibrational properties of the material and verify if they reproduce the experimental results. As a test network, we used the 64 atoms sample of Fig. 1. This sample has 18 sp^2 bonded atoms and the others are sp^3 coordinated. This model was generated in Ref. [12] using tight-binding molecular dynamics.

In order to test the electronic structure of our network, we calculated the Electronic Density Of States (EDOS) and the electronic susceptibility $\chi(\omega_L)$. The EDOS in Fig. 2(A) shows two maxima, above and below the Fermi energy. These peaks correspond to the σ and σ* states. Two smaller and sharper peaks are present at the edges of the band gap. They correspond to the π and π* states generated by the sp^2 bonds. Some sp^2 defect states are present in the band gap, which is of 1.4 eV. This gap is smaller than experimental ta-C, but consistent with that usually found for simulated samples, which systematically underestimate it. It is not due to any inaccuracy in the computational procedure nor to an unrealistic network geometry.

Fig. 2(B) plots the dielectric function $\varepsilon(\omega_L)=1+4\pi\chi(\omega_L)$. Re[$\varepsilon(0)$] is 5.8, in good agreement with the typical values experimentally measured in ta-C [19–21]. Three sharp peaks are present in the imaginary part of the susceptibility. They correspond to three discontinuities in the Re[$\varepsilon(\omega_L)$]. These features are due to the presence of π defect states in the gap,

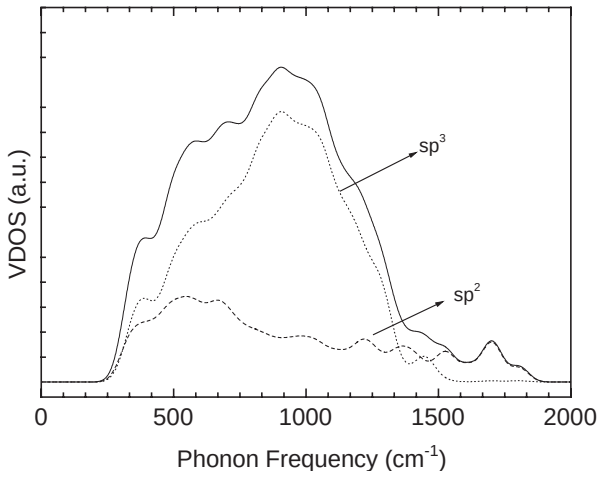

Fig. 3. Calculated vibrational density of states of the sample in Fig. 1. The partial sp^2 and sp^3 contribution are also shown.

and are artefacts due to the small number of atoms in the network. The peaks in Im[$\varepsilon(\omega_L)$] correspond to electronic transitions between the defect states in the gap. They thus give an anomalous absorption of radiation with an energy of 1.3, 2.9 and 4.9 eV. If we neglect the defect states in the computation of $\varepsilon(\omega_L)$, this gives no peaks and a smooth dependence of the susceptibility on the excitation energy.

Fig. 3 plots the Vibrational Density Of States (VDOS) of the sample. The density of normal modes, ranging from ~300 to ~1800 cm^{-1}, is centred at ~1000 cm^{-1} and has a bell shape, with a high frequency tail. Fig. 3 also plots the VDOS of the sp^2 and sp^3 phases, which show two distinct behaviours. The total VDOS is clearly dominated by the sp^3 contribution, however no sp^3 contribution is present for frequencies above 1500 cm^{-1}. On the other hand, sp^2 modes are present in the whole range of the network vibration frequencies and they have an almost constant density, which only shows a weak maximum at ~500 cm^{-1}. It is clear that the VDOS in Fig. 3 does not resemble at all the measured Raman spectra and it is not possible to use it to identify the Raman features as often done in previous papers. In order to directly compare it with the experimental results, it is necessary to "dress" the VDOS with the mode susceptibility at a given excitation energy.

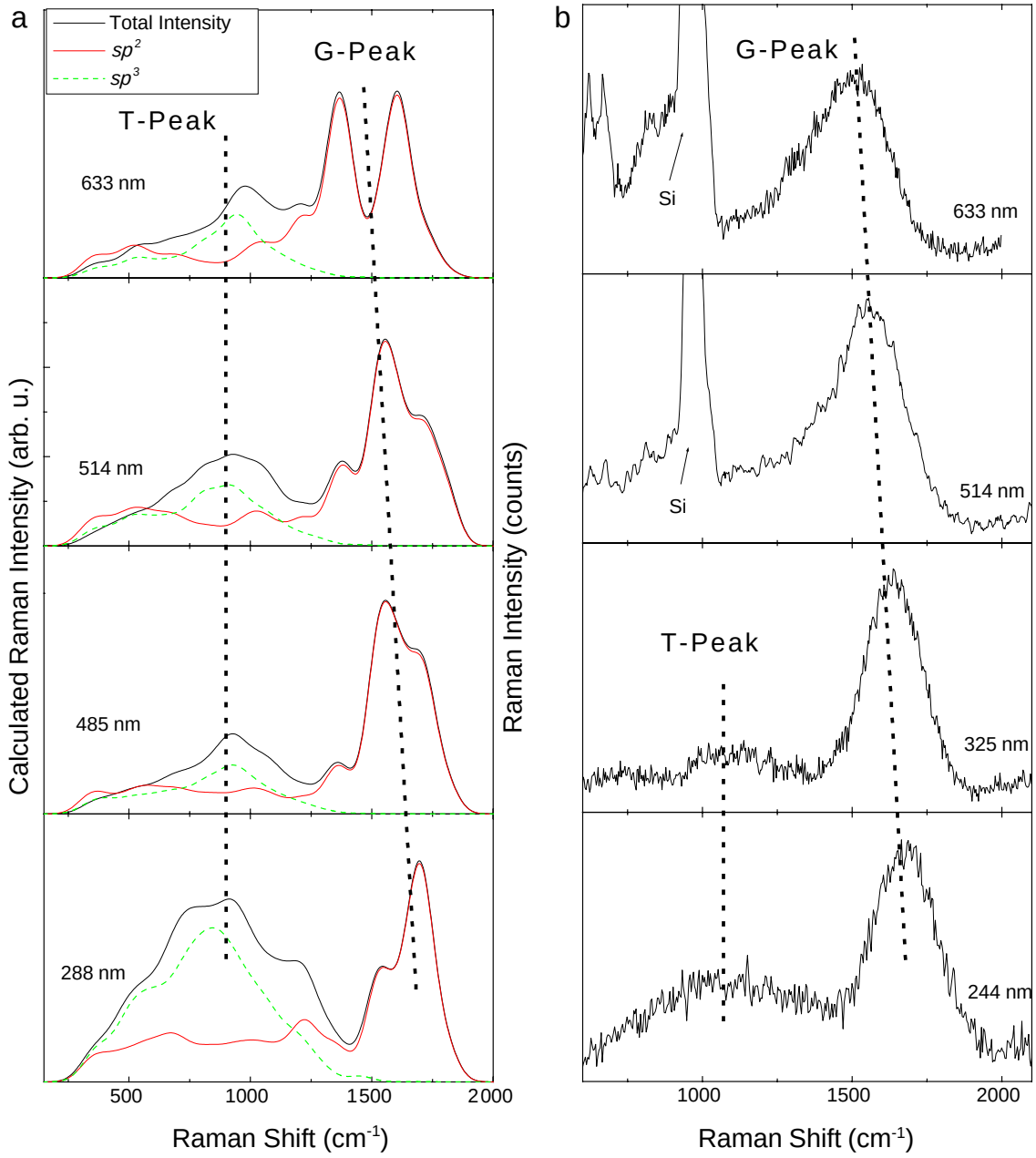

Fig. 4. (a) Calculated Raman spectra for a set of different excitation wavelengths for the model ta-C sample shown in Fig. 1. The total Raman spectra are decomposed in the contributions from sp^2 and sp^3 atoms. The double peak structure of the G peak is an artefact due to the small number of sp^2 sites in the model ta-C. (b) Experimental multi-wavelength Raman spectra of ta-C.

We thus calculate the Raman spectra of the ta-C network in the 785–229 nm excitation range, chosen to match the range of the experimental Raman measurements on ta-C [9], Fig. 4a. The Raman spectra have not been calculated for the excitation energies corresponding to the peaks of $\mathrm{Im}[\varepsilon(\omega_L)]$.

A key parameter in resonant Raman scattering is the difference between the excitation energy and the possible real electronic transitions. Since our calculations underestimate the electronic gap, the resonant spectral features are expected to occur for energies slightly lower than the experimental ones. Fig. 4b plots the experimental Raman spectra of a ta-C film measured for different laser excitation wavelengths from the visible to the UV [9]. The dependence of the G peak position on the excitation wavelength is evident just by eye inspection both in the calculated and in the experimental spectra. The experimental spectra show the extra T peak only for UV excitation. The second order of the Si substrate is also seen for visible excitation, due to the transparency of the thin ta-C sample to visible wavelengths.

Fig. 4(a) plots the calculated spectra. We calculated the Raman intensity of every normal mode of the network. The small number of atoms (64) in our system implies that the Raman spectrum is discrete. Indeed, if N is the number of atoms, the number of normal modes is $3N$. Every mode has its own Raman cross-section and contributes to the total Raman intensity. For a very large number of atoms, such as a real ta-C film, the resulting Raman spectrum is continuous. On the other hand, for a few atoms structure the spectrum is discrete. In order to obtain a continuous Raman spectrum, to be compared with the experimental ones, the contributions of the discrete vibrational eigenmodes have been broadened with a Gaussian. This smoothens the calculated spectrum, but due to the very small number of sp^2 atoms, the G peak still shows a bimodal shape. It is interesting to note, however, that the low-energy sp^2 modes in the G peak decrease with excitation energy, whilst the intensity of the high-energy sp^2 modes increases.

Fig. 4 shows that our calculated spectra reproduce all the main features of the experimental spectra. In particular, the shift of the average G peak position with excitation energy (G peak dispersion) is clear. Also, the increase of the T peak intensity with excitation energy is evident. In our simulations the T peak intensity appears to be always higher than the experimental one. This can be explained considering that

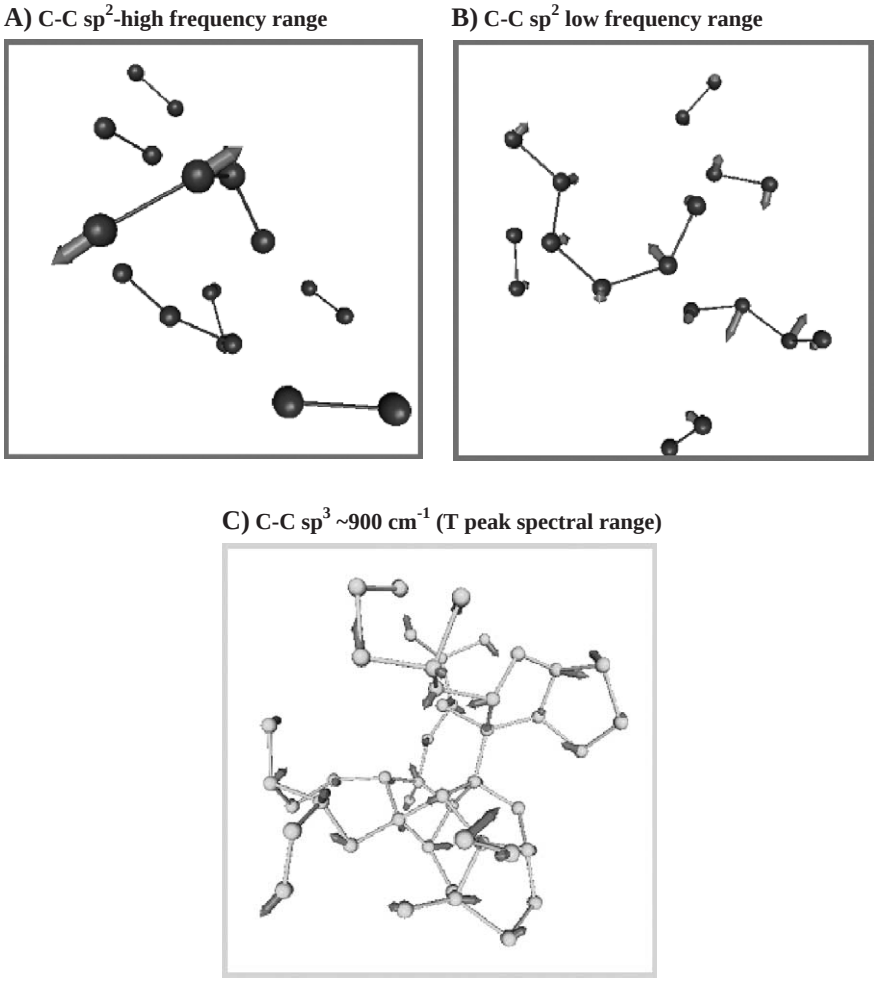

Fig. 5. Representative (A,B) sp^2 and (C) sp^3 modes across the spectral range of a typical ta-C Raman spectrum.

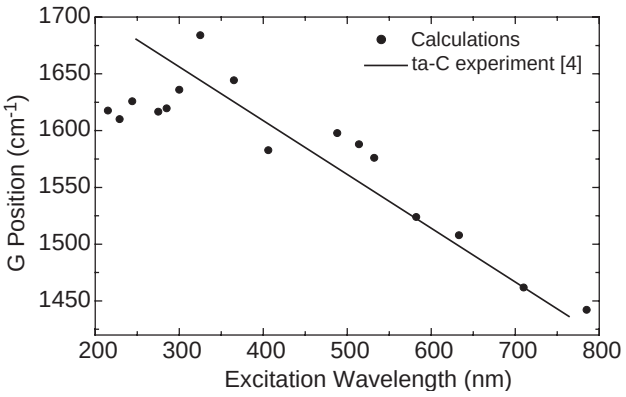

Fig. 6. Comparison between the experimental and the calculated G peak dispersions.

our underestimated gap makes resonance occur at slightly lower energies than the experimental ones.

We further decomposed the calculated spectra to separate the sp^2 and sp^3 contributions, Fig. 4a. This clearly proves that the G peak, which is the main spectral feature of the ta-C spectrum, is *entirely* due to vibrations of sp^2 atoms. It is also evident that for UV excitation, the T peak closely resembles the density of states of the sp^3 bonded atoms, confirming the original assignment of this peak [7,8].

The analysis of the pattern of the vibrational eigenmodes shows that the modes associated to the G peak are due to bond stretching between sp^2 atoms. These involve the motions of very few atoms and are easily distinguishable from the low frequency sp^2 vibrations, which involve motions of all atoms of all the sp^2 clusters in the network. Fig. 5 plots a set of representative sp^2 and sp^3 modes across the 300–1800 cm^{-1} frequency range.

By fitting our calculated spectra in a similar way to that done for the experimental fits, we derive the dispersion of the G peak, and compare it with a typical experimental dispersion, Fig. 6. The agreement between theory and experiment is good. For high excitation energies, the theoretical dispersion tends to saturate. Due to the gap underestimation, this corresponds to an excitation energy range higher than the maximum so far probed experimentally. The saturation of the G peak dispersion for very high excitation energies however is not surprising. This is expected to occur when the excitation energy is higher than the highest local gap cluster [9]. By further increasing the energy, the resonance conditions do not change anymore.

Calculations on networks with lower sp^3 contents are consistent with the experimentally found decrease of the G peak dispersion [9]. However, in order to properly treat the sp^2 phase when rings are present we need to improve the code used for ta-C, which contains only olefinic sp^2 chains, in order to take into account the peculiar resonant nature of the D peak [4,6]. This is underway and will be reported elsewhere.

4. Conclusions

We presented a model for the calculations of resonant Raman spectra of carbon films. We calculated the Raman spectra for a number of different excitation energies on a model ta-C sample. Our calculations reproduce well the main experimental findings, such as the G-peak dispersion as a function of excitation energy, the sp^2 nature of the G peak and the appearance of a C–C sp^3 T-peak for UV excitation.

Acknowledgements

Calculations were performed at HPCF (Cambridge) and IDRIS (Orsay) using CPMD. S.P. was supported by the EU project FAMOUS and the Marie Curie Fellowship IHP-HPMT-CT-2000-00209. A.C.F. acknowledges funding from the Royal Society.

References

[1] J. Robertson, Math. Sci. Eng. R 37 (2002) 129;
A.C. Ferrari, Surf. Coat. Technol. 180-181 (2004) 190.
[2] A.C. Ferrari, J. Robertson, Phys. Rev., B 61 (2000) 14085;
A.C. Ferrari, J. Robertson (Eds.), *Raman spectroscopy in carbons: from nanotubes to diamond*, Phil. Trans. Roy. Soc. A, vol. 362, 2004, Theme Issue, 2267–2565.
[3] F. Tuinstra, J.L. Koening, J. Chem. Phys. 53 (1970) 1126.
[4] C. Thomsen, S. Reich, Phys. Rev. Lett. 85 (2000) 5214.
[5] C. Castiglioni, E. Di Donato, M. Tommasini, F. Negri, G. Zerbi, Synth. Met. 139 (2003) 885.
[6] S. Piscanec, M. Lazzeri, F. Mauri, A.C. Ferrari, J. Robertson, Phys. Rev. Lett. 93 (2004) 185503.
[7] K.W.R. Gilkes, H.S. Sands, D.N. Batchelder, J. Robertson, W.I. Milne, Appl. Phys. Lett. 70 (1997) 1980.
[8] V.I. Merkulov, J.S. Lannin, C.H. Munro, S.A. Asher, V.S. Veerasamy, W.I. Milne, Phys. Rev. Lett. 78 (1997) 4869.
[9] A.C. Ferrari, J. Robertson, Phys. Rev., B 64 (2001) 075451.
[10] A.C. Ferrari, S.E. Rodil, J. Roberston, Phys. Rev., B 67 (2003) 155306.
[11] R. Loudon. The quantum theory of light. 1983, Clarendon Press and Oxford University Press, New York.
[12] D.A. Drabold, P.A. Fedders, P. Stumm, Phys. Rev., B 49 (1994) 16415.
[13] G. Placzek, in: E. Marx (Ed.), Handbuch der Radiologie, vol. 6, Akademische Verlagsgesellschaft, Leipzig, 1934, p. 209.
[14] M. Profeta, F. Mauri, Phys. Rev., B 63 (2001) 245415.
[15] S. Baroni, S. De Gironcoli, A. Dal Corso, P. Giannozzi, Rev. Mod. Phys. 73 (2001) 515.
[16] J. Hutter, P. Ballone, M. Bernasconi, P. Focher, E. Fois, S. Goedecker, D. Marx, M. Parinello, M. Tuckerman, CPMD Version 3.3.5, (MPI fur Festkorperforschung and IBM Research Laboratory, 1990–1998).
[17] N. Troullier, J.N. Martins, Phys. Rev., B 43 (1991) 1993.
[18] H. Xu, C.Z. Wang, C.T. Chan, K.M. Ho, J. Phys., Condens. Matter 4 (1992) 6047.
[19] Y. Lifshitz, et al., Diamond Relat. Mater. 6 (1997) 687.
[20] Z.Y. Chen, J.P. Zhao, J. Appl. Phys. 87 (2000) 4268.
[21] A.C. Ferrari, A. Li Bassi, B.K. Tanner, V. Stolojan, J. Yuan, L.M. Brown, S.E. Rodil, B. Kleinsorge, J. Robertson, Phys. Rev., B 62 (2000) 11089.